ChemPubSoc Europe

DOI: 10.1002/chem.201504328

CHEMISTRY A European Journal Full Paper

Chalcogens |*Hot Paper*|

Supramolecular Wiring of Benzo-1,3-chalcogenazoles through Programmed Chalcogen Bonding Interactions

Adrian Kremer,[a] Andrea Fermi,[a] Nicolas Biot,[a, c] Johan Wouters,[a] and Davide Bonifazi*[a, b, c]

Abstract: The high-yielding synthesis of 2-substituted benzo-1,3-tellurazoles and benzo-1,3-selenazoles through a dehydrative cyclization reaction has been reported, giving access to a large variety of benzo-1,3-chalcogenazoles. Exceptionally, these aromatic heterocycles proved to be very stable and thus very handy to form controlled solid-state organizations in which wire-like polymeric structures are formed through secondary N···Y bonding interactions (SBIs) engaging the chalcogen (Y = Se or Te) and nitrogen atoms. In particular, it has been shown that the recognition properties of the chalcogen centre at the solid state could be programmed by selectively barring one of its σ-holes through a combination of electronic and steric effects exerted by the substituent at the 2-position. As predicted by the electrostatic potential surfaces calculated by quantum chemical modelling, the pyridyl groups revealed to be the stronger chalcogen bonding acceptors, and thus the best ligand candidate for programming the molecular organization at the solid state. In contrast, the thiophenyl group is an unsuitable substituent for establishing SBIs in this molecular system as it gives rise to chalcogen–chalcogen repulsion. The weaker chalcogen donor properties of the Se analogues trigger the formation of feeble N···Se contacts, which are manifested in similar solid-state polymers featuring longer nitrogen–chalcogen distances.

Introduction

The concept of secondary bonding interactions (SBIs) describes interactions resulting from interatomic contacts that are longer than the covalent single bonds but shorter than the sum of van der Waals radii.[1,2] Depending on the context, these interactions have been also called soft-soft, closed-shell, nonbonding, semi-bonding, non-covalent, weakly bonding, or σ-hole-interactions.[3,4] Formally, a secondary bond derives from a n^2(X)→σ*(Y-electron withdrawing group (EWG)) donation, in which the lone pair of an electro-donating atom X interacts with an antibonding σ* orbital of a Y-EWG bond, in which Y and EWG stand for the polarizable atom and electron withdrawing group, respectively. Typically, this is described by an σ-hole, a region of positive electrostatic potential located on the Y atom at the opposite side of the Y-EWG bond. Descending the periodic table, the polarisability of atoms increases reducing the difference between the energy levels of the σ(Y-EWG) and σ*(Y-EWG) molecular orbitals, thus favouring stronger SBIs. Halogen bonding is certainly the most investigated interactions of this class,[5–7] and its importance has been recently demonstrated in different domains, ranging from materials to biological applications.[8–16]

We can extend this type of interaction to all molecular structures in which an electron-deficient polarizable atom is present. This includes electron-deficient chalcogen atoms, which are known to form X···Y-EWG SBIs in the solid state[4,17–20] and in solution.[21] Considering the experimental evidences and the theoretical studies,[22–27] strong SBIs can be expected when descending in the chalcogen group, with the Te-derived compounds establishing the strongest interactions.[21] Among the different chalcogenide derivatives, benzo-2,1,3-telluradiazoles have certainly attracted the greatest interest because of their unique ribbon-like self-organization in the solid state (Figure 1 a) formed through strong N···Te SBIs (2.682(7)–2.720(7) Å).[4,28–31] Although of great potential, these molecular systems have remained confined to the fundamental research because of their thermal instability and aptitude to undergo hydrolysis under ambient conditions.

In contrast, although 2-substituted benzo-1,3-tellurazoles are more chemically inert that their parent benzo-2,1,3-chalcogenadiazoles, they have been only marginally studied for preparing self-organized functional materials. Only in the late 1980s[32] was the first and only X-ray structure of a 2-sustituted benzo-1,3-tellurazole described. In the solid state, the molecule organizes into wires held by intermolecular N···Te contacts (Fig-

[a] *Dr. A. Kremer, Dr. A. Fermi, N. Biot, Prof. J. Wouters, Prof. Dr. D. Bonifazi*
Namur Research College (NARC) and Department of Chemistry
University of Namur (UNamur), Rue de Bruxelles 61, Namur, 5000 (Belgium)

[b] *Prof. Dr. D. Bonifazi*
Department of Pharmaceutical and Chemical Sciences
and INSTM UdR Trieste
University of Trieste, Piazzale Europa 1, Trieste 34127 (Italy)

[c] *N. Biot, Prof. Dr. D. Bonifazi*
School of Chemistry, Cardiff University, Park Place, CF10 3AT, Cardiff (UK)
E-mail: BonifaziD@cardiff.ac.uk

Supporting information for this article is available on the WWW under http://dx.doi.org/10.1002/chem.201504328.

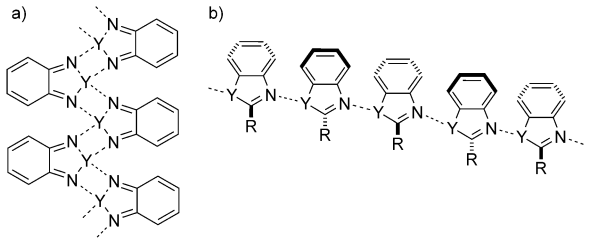

Figure 1. Solid-state arrangements of a) benzo-2,1,3-telluradiazoles and b) benzo-1,3-tellurazole in tapes and wires, respectively.

ure 1 b).[32] A similar wire-like organization was also recently reported by us with a phosphorescent 2-substituted ethynylbenzotellurazole.[33] Given these premises and considering the ease of tuning their chemical and physical properties with simple chemical modifications of the benzo ring, 2-substituted benzo-1,3-chalcogenazoles can be privileged heterocyclic systems to engineer soft materials featuring wire-like arrangement at the molecular scale. To shed further light on the use of X···Y SBIs (Y = Se or Te) for mastering the supramolecular arrangement at the solid state, we have developed a versatile protocol to prepare 2-substituted benzo-1,3-selenazoles and benzo-1,3-tellurazoles bearing alkyl, alkenyl, aryl and heteroaryl groups in high yields. The solid-state arrangement shows that, depending on the electronic and geometrical properties of the substituent at the 2-position, one can control the wiring organization through two- (X···Y) or three-atoms (X···Y···X) SBIs.

Results and Discussion

Programming the benzo-1,3-chalcogenazole synthons

Provided that a sufficiently basic heteroatom (X) is present in the molecular structure of a substituted chalcogenazole, one can expect to control the organization at the solid state of functional molecular synthons through selected X···Y SBIs. In particular, programmed supramolecular wire-like polymers could be formed at the solid state, exploiting SBIs other than those established through the chalcogenazole N atom. To appraise the possibility of programming the benzo-1,3-chalcogenazoles for controlling the solid-state arrangements through chalcogen SBIs, we used electrostatic surface potentials (ESP). As described recently by Taylor and co-workers,[21] it is well accepted that an estimation of the ability to make X···Y SBIs can be obtained considering the magnitude of $V_{s,max}$ at X and Y atoms (i.e., the value of the electrostatic potential at the point of the highest charge for both donor and acceptor atoms),[21–27] although the chalcogen bonding interactions cannot be considered as purely electrostatic interactions.[34–38] Calculations have been firstly performed on non-substituted benzo-1,3-chalcogenazoles using Gaussian 09 including the D01 Revision, with the B97-D3/Def2-TZVP level of theory.[21] After geometry optimization, the ESPs were mapped on the van der Waals surface of each molecule up to an electron density of 0.001 electron bohr^{-3}. $V_{s,max}$ was determined with a classical method.[39] As previously observed for benzo-2,1,3-chalcogenadiazoles,[21] two electron deficient regions (σ-holes) centred at the chalcogen Y atom, each situated at the terminus of the C–Y bond, could be evidenced from the ESP surfaces. In contrast to benzo-2,1,3-telluradiazoles, both benzo-1,3-selenazole and benzo-1,3-tellurazole features σ-holes displaying different $V_{s,max}$ values (Figure 2 a).

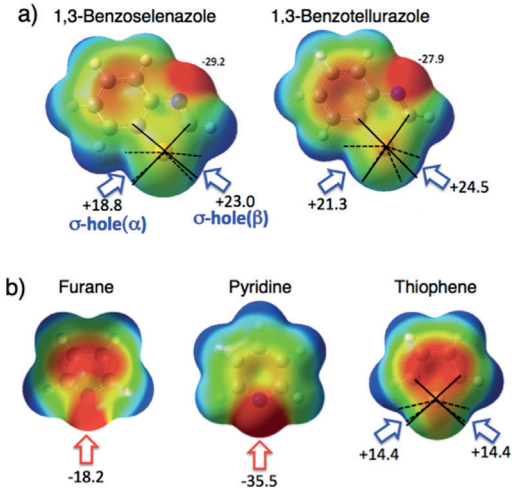

Figure 2. ESP (kcal mol^{-1}, calculated using Gaussian 09 at B97-D3/def2-TZVP level of theory) for a) unsubstituted chalcogenazoles displaying the two σ-holes (labelled as α and β, respectively) and b) furanyl, pyridyl and thiophenyl ligands. The red and blue indicate negative and positive charge densities.

To distinguish the σ-holes, the following terminology will be used throughout this manuscript: σ-hole(α) and σ-hole(β) for describing positive electrostatic regions on the chalcogen atom exposed on the side of the 4- and 2-positions, respectively (Figure 2 a). The calculated $V_{s,max}$ values for benzo-1,3-selenazole are +18.8 and +23.0 kcal mol^{-1} for the α and β σ-holes, respectively (Figure 2). Similar values were also obtained for benzo-1,3-tellurazole, +21.3 and +24.5 kcal mol^{-1} for the α and β σ-holes, respectively. This suggests that both benzo-1,3-chalcogenazoles are suitable molecular synthons to undergo SBI recognition. Although the differences in the $V_{s,max}$ values between the two σ-holes are very small, the σ-hole(β) in non-substituted benzo-1,3-chalcogenazoles features slightly higher electrostatic values, possibly anticipating selectivity in the recognition mode. Instead, the N atom of the chalcogenazole features the most negative $V_{s,max}$ values (−29.2 and −27.9 kcal mol^{-1}, for the Se and Te derivatives, respectively), making it the strongest basic site and thus a privileged acceptor atom for establishing a chalcogen bonding interaction. This behaviour has been confirmed with 2-phenyl benzo-1,3-tellurazole at the solid state.[32] Conversely, if we want to control the supramolecular architecture with SBIs engaging a different atom than the N of the chalcogenazole, we have to use ligands featuring basic sites with higher negative $V_{s,max}$ values. Among the different acceptors, we have focused our attention on the pyridyl, furanyl and thiophenyl aromatic rings. Whereas the calculated $V_{s,max}$ values are −18.2 and −35.5 kcal mol^{-1} for the O and N atoms of the furane and pyridine structures, respectively

(Figure 2b), the thiophenyl ring displays an ESP distribution on the S atom similar to that of the chalcogenazoles. Namely, two σ-hole electron-deficient regions centred on the S atom, each situated at the termini of the S–C bonds, are evident in the ESP (Figure 2b). In particular, a calculated $V_{s,max}$ value of $+14.4$ kcal mol^{-1} has been obtained suggesting that the S atom does not present the favourable electrostatic properties for engaging the Se or Te atoms in an in-plane SBI. Therefore it is evident that the chalcogen-bonding acceptor abilities that can be inferred from the calculated $V_{s,max}$ designates the pyridyl moiety as the best ligand, followed by the chalcogenazole and furanyl rings. Instead, the thiophenyl rings is expected to establish in-plane repulsive interactions.

Indulging these computational results, we prepared benzo-1,3-chalcogenazoles bearing different pyridyl, furanyl and thiophenyl moieties at the 2-position to tailor the recognition properties of the chalcogen atom and to control the supramolecular organization at the solid state. Specifically, it is envisaged that the self-assembly behaviour of benzo-1,3-chalcogenazoles can be mastered by programming the 2-position with suitable functional groups through a) steric hindrance (Figure 3a), b) electrostatic stopping (Figure 3b), or c) intermolecular tethering (Figure 3c). This can result in either tuning the recognition properties of the chalcogen atom (a and b) or governing the formation of different supramolecular arrangements (c). As anticipated above, particular attention will be given to the introduction of substituents at the 2-position with suitable electronic and geometrical requirements to master the formation of supramolecular wires featured through two- (X···Y) or three-atoms (X···Y···X) SBIs.

Synthesis

Only a limited number of reports are described in the literature about the preparation of 2-functionalised benzoselenazole derivatives bearing in 2-position an alkyl, aryl or heteroaryl substituent (Scheme 1). A first approach is the dehydrative cyclization of 2-selenoanilides reported in the 1980s by Christiaens and co-workers, who prepared a few benzoselenazoles and tellurazoles derivatives by cyclization of 2-chalcogenoanilides with $POCl_3$ (route a).[40]

Nevertheless, the extremely low yield (≈1%, over the four steps synthesis), the use of extremely evil-smelling and toxic reagents (e.g., Et_2Te_2), the low chemical versatility, and contradictory reports about reproducibility issues,[41] limited the scope of the original protocol. Following reports by Minkin and co-workers showed that 2-methyl- and 2-phenyl-substituted benzotellurazoles could be obtained by cyclization of 2-telluroanilides in neat $POCl_3$ with improved yields.[42,43] However, the harsh acidic conditions severely narrow the compatibility of the protocol to a limited family of substrates. Recently, two new synthetic routes toward the preparation of alkyl-, aryl- and heteroaryl-substituted derivatives have been developed (routes b and d). In route b,[44–46] bis(2-aminophenyl)diselenide is reacted with a carbonyl derivative in the presence of a reducing agent, whereas the second approach exploits Woollins' reagent and 2-iodoanilides (route c).[47] Finally, a copper-catalysed three-component one-pot synthesis, limited to the case of aryl and heteroaryl derivatives, has been described very recently (route d).[48] In the case of the benzotellurazoles analogues, the synthetic protocols are scarcer.[40–43,49–51] To the best of our knowledge, the developed methods to date (Scheme 2) are limited to the preparation of 2-substituted alkyl and aryl derivatives. This exploits the dehydrative cyclization of 2-telluroanilides with either phosphorus oxychloride,[40,42,43,49] phosphorus trichloride[41] or hypophosphorus acid,[50,51] with the latter conditions only compatible for the synthesis of alkyl and aryl 2-substituted derivatives.

Inspired by the synthetic route developed by Christiaens and co-workers,[40] we focused our attention on the dehydra-

Figure 3. Programming the recognition properties of benzo-1,3-chalcogenazoles through a) hindering, b) stopping or c) tethering the σ-holes.

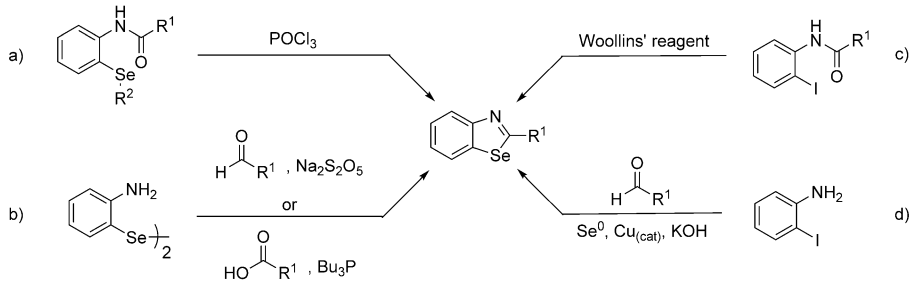

Scheme 1. The different synthetic approaches toward the preparation of 2-functionalised benzoselenazole derivatives starting from: a) 2-selenoanilides (R_1 = Me or aryl; R_2 = Me or Et);[40] b) bis(2-aminophenyl)diselenide (R_1 = alkyl or aryl);[44,45] c) 2-iodoanilides (R^1 = alkyl, aryl or heteroaryl); and[47] d) 2-iodoaniline (R_1 = aryl or heteroaryl).[48]

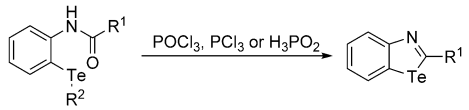

Scheme 2. Synthetic approach for the preparation of 2-functionalised benzotellurazole derivatives (R^1 = alkyl or aryl).[40–43,49–51]

tive cyclization reaction to prepare the targeted 2-substituted chalcogenazole derivatives. Starting from *o*-methylseleno- ($\mathbf{1_{Se}}$) and *o*-methyltelluro-aniline ($\mathbf{1_{Te}}$), prepared in two steps from 2-bromoaniline,[33] we have synthesized a series of selenoanilides ($\mathbf{2_{Se}}$–$\mathbf{10_{Se}}$) and telluroanilides ($\mathbf{2_{Te}}$–$\mathbf{10_{Te}}$) with very good yields (Table 1, first step) upon reaction with the appropriate acyl chloride. Adapting the protocol by Minkin[42,43] to milder reaction conditions, anilides $\mathbf{2_Y}$–$\mathbf{10_Y}$ could be converted into targeted benzoselenazoles and tellurazoles $\mathbf{11_Y}$–$\mathbf{19_Y}$ in very good to excellent yields in less than three hours (Table 1, second step, entries 1–14 and 17 and 18) using two equivalents of $POCl_3$ in the presence of Et_3N heated at reflux in 1,4-dioxane.[42,43] The only exception was restricted to the cases of picolinamide derivatives $\mathbf{9_Y}$, which were transformed into the 2-(pyridin-2-yl)-benzochalcogenazole derivatives, $\mathbf{18_{Se}}$ and $\mathbf{18_{Te}}$, in modest yields (Table 1, entries 15 and 16).

As anticipated above, the protocol is compatible with a wide range of substituents in the 2-position. Indeed, alkyl (Table 1, entries 1 and 2) and alkenyl (Table 1, entries 5 and 6) moieties were successfully inserted, as well as aromatic (Table 1, entries 3 and 4) and heterocyclic substituents, like furanyl, thiophenyl, pyridyl and ferrocenyl moieties (Table 1, entries 7–18). All structures were fully characterized by ^{1}H- and ^{13}C NMR spectroscopy and HR-Mass spectrometry. We also performed complementary ^{125}Te-NMR analyses on the tellurazoles. All spectra display a singlet with similar chemical shifts in the spectral region between $\delta = 852$ and 892 ppm, with the 2-phenyl and 2-*i*-butyl tellurazoles exhibiting the two limiting values, respectively (Table 2). Because of the N atom in the 3-position, the ^{125}Te chemical shifts are significantly deshielded with respect to reference Ph_2Te_2, in agreement with the literature reports.[41,50,52,53] Considering that the coordination of a Te atom can result in upfield shifts as big as $\delta = 200$ ppm,[52,53] the ^{125}Te-NMR measurements are not conclusive to support the existence of any inter- or intramolecular SBIs in solution.

Table 2. ^{125}Te NMR chemical shifts in $CDCl_3$ solution at 293 K (reference taken with Ph_2Te_2).

Compounds	$\mathbf{11_{Te}}$	$\mathbf{12_{Te}}$	$\mathbf{14_{Te}}$	$\mathbf{15_{Te}}$	$\mathbf{16_{Te}}$	$\mathbf{17_{Te}}$	$\mathbf{18_{Te}}$
δ (^{125}Te, $CDCl_3$) [ppm]	892	852	884	877	884	870	874

Table 1. Two-step synthesis for preparing 2-substituted chalcogenazoles from 2-chalcogenoanilides by dehydrative cyclization. Y = Se or Te.

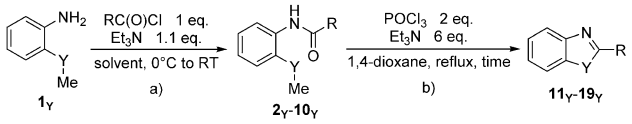

$\mathbf{1_Y}$ → $\mathbf{2_Y}$-$\mathbf{10_Y}$ → $\mathbf{11_Y}$-$\mathbf{19_Y}$

Entry	R	Y	a) Product	a) Yield [%][a]	a) *t* [h]	b) Product	b) Yield [%][a]
1	*i*Bu	Se	$\mathbf{2_{Se}}$	90	3	$\mathbf{11_{Se}}$	77
2		Te	$\mathbf{2_{Te}}$	87	3	$\mathbf{11_{Te}}$	84
3	Ph	Se	$\mathbf{3_{Se}}$	95	3	$\mathbf{12_{Se}}$	88
4		Te	$\mathbf{3_{Te}}$	94	3	$\mathbf{12_{Te}}$	83
5	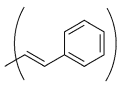	Se	$\mathbf{4_{Se}}$	64	3	$\mathbf{13_{Se}}$	90
6		Te	$\mathbf{4_{Te}}$	70	3	$\mathbf{13_{Te}}$	86
7		Se	$\mathbf{5_{Se}}$	84	3	$\mathbf{14_{Se}}$	88
8		Te	$\mathbf{5_{Te}}$	75	3	$\mathbf{14_{Te}}$	96
9		Se	$\mathbf{6_{Se}}$	90	3	$\mathbf{15_{Se}}$	87
10		Te	$\mathbf{6_{Te}}$	94	3	$\mathbf{15_{Te}}$	91
11		Se	$\mathbf{7_{Se}}$	88	3	$\mathbf{16_{Se}}$	87
12		Te	$\mathbf{7_{Te}}$	66	1.5	$\mathbf{16_{Te}}$	88
13		Se	$\mathbf{8_{Se}}$	98	2	$\mathbf{17_{Se}}$	66
14		Te	$\mathbf{8_{Te}}$	93	1.5	$\mathbf{17_{Te}}$	80
15		Se	$\mathbf{9_{Se}}$	98	8[b]	$\mathbf{18_{Se}}$	39[b]
16		Te	$\mathbf{9_{Te}}$	90	6[c]	$\mathbf{18_{Te}}$	67[c]
17		Se	$\mathbf{10_{Se}}$	55	3	$\mathbf{19_{Se}}$	81
18		Te	$\mathbf{10_{Te}}$	59	3	$\mathbf{19_{Te}}$	81

[a] Yield of the isolated product. [b] 83% conversion. [c] 92% conversion.

Recently, the same protocol allowed us to prepare 2-ethynyl benzo-1,3-chalcogenazoles and bisbenzo-1,3-chalcogenazoles.[33] To further show the synthetic versatility of the approach, the preparation of trisbenzo-1,3-selenazole $\mathbf{21_{Se}}$ and −1,3-tellurazole $\mathbf{21_{Te}}$ was also attempted (Scheme 3). Treatment of anilines $\mathbf{1_Y}$ with 1,3,5-benzenetricarbonyl trichloride in the presence of Et_3N gave trisanilides $\mathbf{20_Y}$. Subsequent cyclization of $\mathbf{20_Y}$ using six equivalents of $POCl_3$ in the presence of Et_3N under reflux in 1,4-dioxane, afforded targeted trisbenzo-1,3-chalcogenazoles $\mathbf{21_Y}$ in very good yields. Both Se and Te trisbenzo-1,3-chalcogenazoles were characterized by mass spectrometric data (see the Supporting Information), ^{1}H NMR, and IR spectra. Because of its poor solubility, only the ^{13}C NMR spectrum of $\mathbf{21_{Te}}$ could be obtained. All attempts to obtain suitable crystals for X-ray analysis revealed to be fruitless.

Steady-state UV/Vis absorption and emission studies in solution

Comparative absorption spectra of compounds $\mathbf{11_Y}$–$\mathbf{19_Y}$ in CH_2Cl_2 are shown in Figures 4, 5, and 6 (see also the Supporting Information), with the key ab-

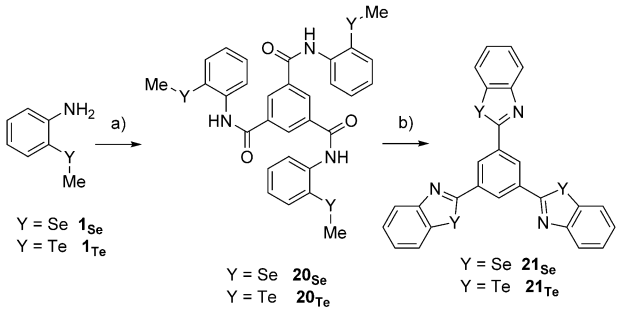

Scheme 3. Synthesis of trisbenzo-1,3-chalcogenazoles $\mathbf{21}_{Se}$ and $\mathbf{21}_{Te}$. Reagents and conditions: a) 1,3,5-benzenetricarbonyl trichloride, Et_3N, CH_2Cl_2, 24 h, RT, Se: 82% of $\mathbf{20}_{Se}$, Te: 57% of $\mathbf{20}_{Te}$; b) $POCl_3$, Et_3N, 1,4-dioxane, time, RT to 102 °C; Se from $\mathbf{20}_{Se}$: 3 h, 72% of $\mathbf{21}_{Se}$, Te from $\mathbf{20}_{Te}$: 3 h, 75% of $\mathbf{21}_{Te}$.

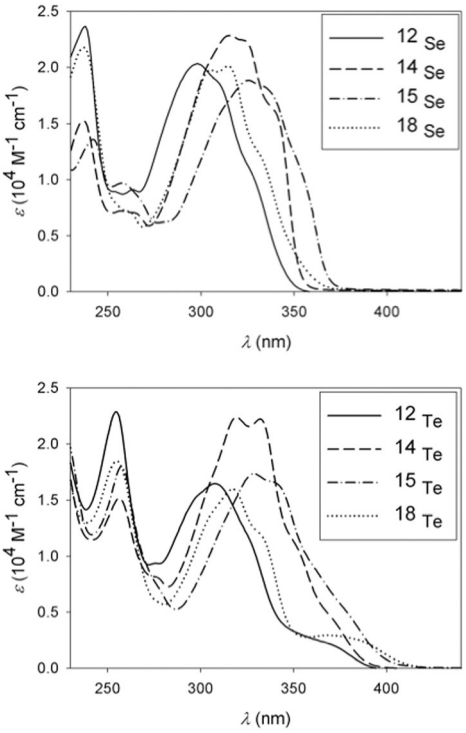

Figure 4. UV/Vis absorption spectra of 2-susbtituted phenyl ($\mathbf{12}_Y$), furanyl ($\mathbf{14}_Y$), thiophenyl ($\mathbf{15}_Y$) and pyridyl ($\mathbf{18}_Y$) benzoselenazoles (top) and benzotellurazoles (bottom) in CH_2Cl_2 at 298 K.

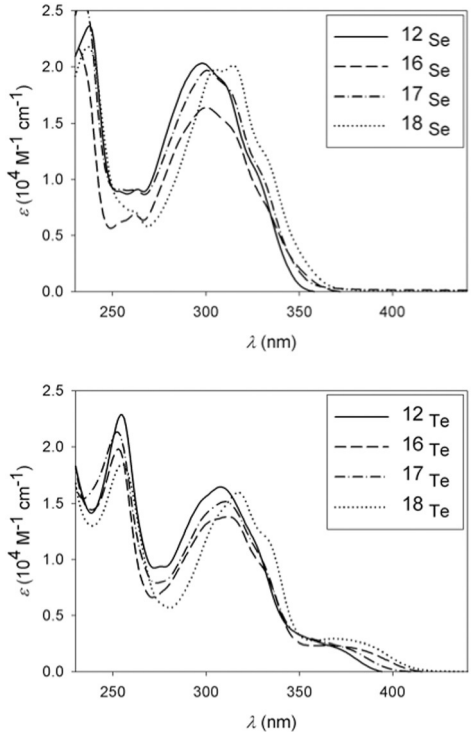

Figure 5. Comparison of the UV/Vis absorption spectra of 2-susbtituted phenyl ($\mathbf{12}_Y$) and the pyridyl ($\mathbf{16}_Y$–$\mathbf{18}_Y$) benzoselenazoles (top) and benzotellurazoles (bottom) in CH_2Cl_2 at 298 K.

Table 3. Absorption parameters of $\mathbf{11}_Y$–$\mathbf{19}_Y$ in CH_2Cl_2 at 298 K.

	λ_{max} [nm] (ε_{max}, 10^3 м$^{-1}$ cm^{-1})	
M	**Se**	**Te**
$\mathbf{11}_Y$	260 (6.8), 292 (2.2), 302 (2.1)	241 (21.3), 260 (9.5), 316 (2.8)
$\mathbf{12}_Y$	238 (23.7), 298 (20.3)	255 (22.9), 308 (16.5), 365 (2.4)
$\mathbf{13}_Y$	272 (7.5), 327 (28.9)	265 (19.0), 335 (29.3), 395 (4.7)
$\mathbf{14}_Y$	238 (15.1), 315 (22.8)	256 (15.2), 320 (22.4), 370 (4.6)
$\mathbf{15}_Y$	242 (13.5), 257 (9.7), 325 (18.9)	258 (17.6), 329 (17.2), 375 (5.5)
$\mathbf{16}_Y$	300 (16.4)	253 (19.8), 310 (13.8), 365 (2.3)
$\mathbf{17}_Y$	301 (19.7)	253 (21.3), 310 (15.2), 365 (2.6)
$\mathbf{18}_Y$	237 (21.8), 305 (19.7), 315 (20.1)	255 (18.5), 318 (16.0), 369 (2.9)
$\mathbf{19}_Y$	304 (15.5), 464 (1.3)	248 (22.9), 309 (14.3), 467 (1.5)

sorption data resumed in Table 3. In general, absorption spectra for compounds $\mathbf{11}_{Se}$–$\mathbf{18}_{Se}$ display a combination of two main bands in the UV region, whereas in the case of the tellurazole analogues ($\mathbf{11}_{Te}$–$\mathbf{18}_{Te}$) an additional electronic transition develops in the visible wavelengths.[33] Differently, $\mathbf{19}_{Se}$ and its analogue $\mathbf{19}_{Te}$ show a broad and low intense absorption band in the visible region, a typical electronic transition fingerprinting the ferrocene unit (Figure 6). For both benzochalcogenazoles, a narrow band is recorded with ε values between 15 000 and 23 000 м$^{-1}$cm^{-1} at higher λ (comprised between 235 and 265 nm), likely corresponding to the electronic transition centred on the phenyl unit. In the presence of an aryl substituent, this transition is slightly redshifted (Figure 4). In the region between 270 nm and 350 nm a broader band is detected for the aryl-substituted benzoselenazoles and benzotellurazoles, showing a vibrational structure only in the case of derivatives $\mathbf{14}_{Te}$ and $\mathbf{15}_{Te}$. Again, this band is redshifted with the progression of the aryl substituents (phenyl > pyridyl > furanyl > thiophenyl) in both chalcogenazole derivatives (Figure 4). Notably, among the pyridyl-substituted chalcogenazoles, only the UV/Vis profiles of $\mathbf{18}_{Se}$ and $\mathbf{18}_{Te}$ are significantly redshifted with respect to the phenyl analogues, probably because of the intramolecular N···Te interaction that planarizes the two heterocyclic moieties (see the X-ray structure in Figure 10). Most likely, the planar conformation significantly increases the π-conjugation between the two aromatic cycles, thus favouring a bathochromic

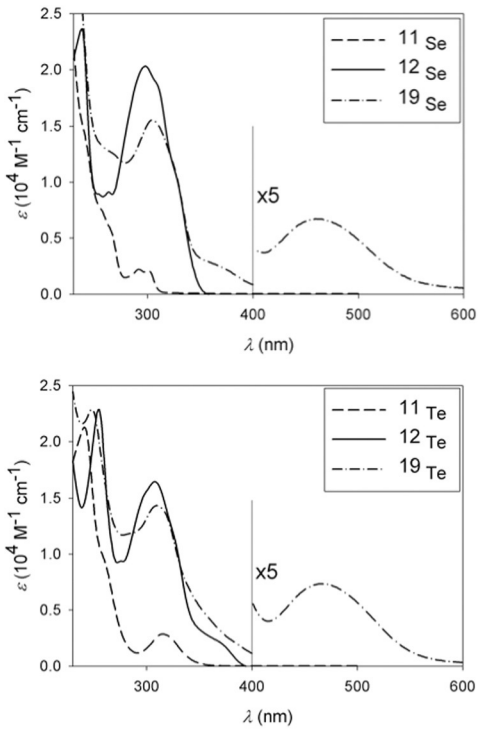

Figure 6. UV/Vis absorption spectra of 2-substituted alkyl- ($\mathbf{11}_Y$), phenyl ($\mathbf{12}_Y$) and ferrocenyl ($\mathbf{19}_Y$) benzoselenazoles (top) and benzotellurazoles (bottom) in CH_2Cl_2 at 298 K.

shift of the electronic transitions. Finally, we can easily notice that the spectra of the benzotellurazole derivatives show a low intensity (between 2500 and 5500 $M^{-1}cm^{-1}$) unstructured band (except for $\mathbf{13}_{Te}$–$\mathbf{15}_{Te}$, in which it appears as a shoulder) that is absent in the absorption profiles of the congener benzoselenazoles.[33] This can be attributed to the presence of the Te atom, which most likely promotes additional $^1n\rightarrow\pi^*$ electronic transition.[54–56]

Luminescence studies of air-equilibrated solutions of benzotellurazoles $\mathbf{11}_{Te}$–$\mathbf{19}_{Te}$ in CH_2Cl_2 at room temperature showed negligible or very low intense ($\Phi < 10^{-3}$) emission profiles, exhibiting no relevant enhancement of the Φ values in de-aerated solutions (after bubbling Ar in the medium for 25 min). On the other hand, 2-pyridyl tellurazole $\mathbf{18}_{Te}$ displays appreciable phosphorus emission only as a powder, with an unstructured band centred at 535 nm (see the Supporting Information). Emission lifetime analysis at 535 nm results in a μs timescale decay ($\tau = 11$ μs), which is compatible with a spin forbidden triplet–singlet deactivation pathway typical of this kind of system, as also recently observed by us with 2-ethynyl benzo-1,3-chalcogenazole derivatives.[33]

Programmed supramolecular organization at the solid state

In this section we will describe the solid-state arrangement of those benzo-1,3-chalcogenazoles that formed crystals suitable for X-ray diffraction (Figures 7–12). In general, all the C–Se, C–Te and N–C bonds belonging to the 1,3-chalcogenazole cores

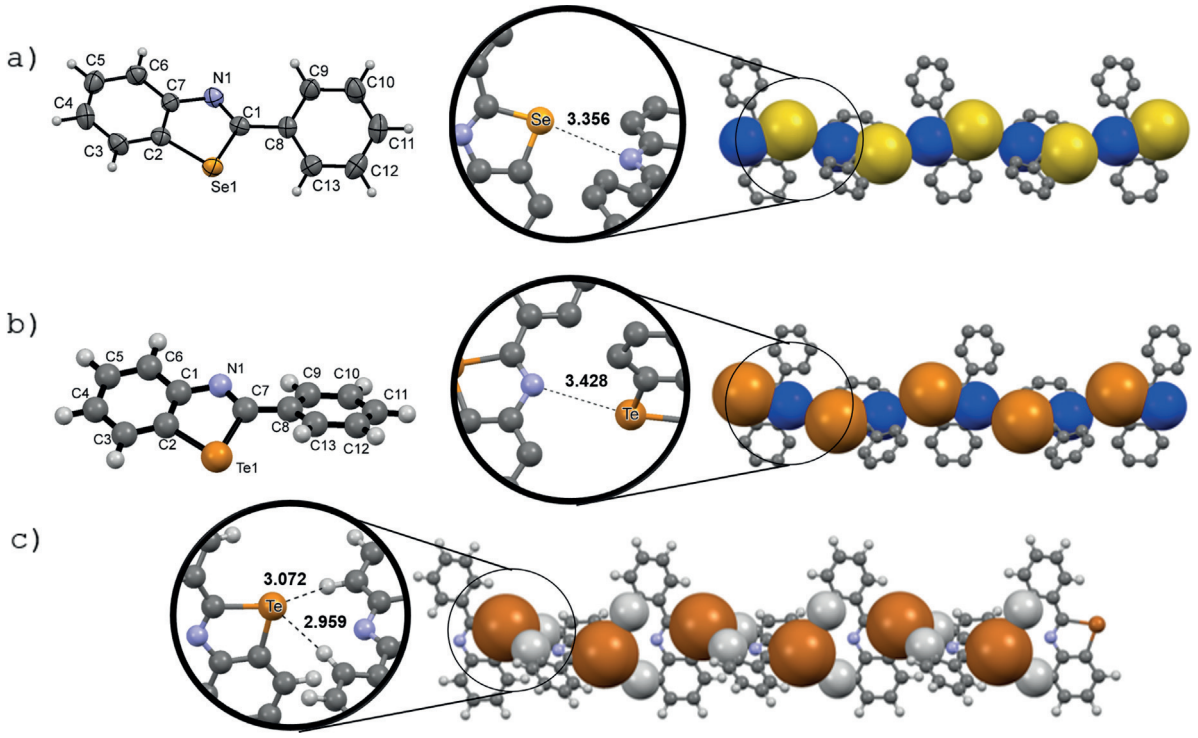

Figure 7. ORTEP (left) and ball-stick representations of the crystal structures of a) $\mathbf{12}_{Se}$ and b) $\mathbf{12}_{Te}$, from which one can evidence the supramolecular wiring motif (the N···Y contacts are viewed with the space-filling model); c) intermolecular interactions between hydrogen and tellurium atoms (C-H···Y) are highlighted with space-filling model representation for crystal structure of $\mathbf{12}_{Te}$. Distances in Å between the chalcogen atom and the SBI donor atoms are highlighted in the inset circles. Space groups: $P2_1/c$ ($\mathbf{12}_{Se}$) and $P2_1/a$ ($\mathbf{12}_{Te}$). Atom colours: blue N, ochre Te, yellow Se, grey C, light grey H.

do not significantly differ between the different molecules bearing the same chalcogen atom. This suggests that the crystal organization does not alter the covalent molecular skeleton. The recognition at the solid-state is discussed considering the molecular conformation (Table 4) and the calculated electrostatic surface potentials (ESP) displayed in the Supporting Information (Table S14). As general principle, one can anticipate that the σ-hole displaying the highest positive $V_{s,max}$ value (Table 5) will be preferentially engaged in the SBI with the functional group bearing the most negative heteroatom.[21,57,58]

Table 4. Experimental and theoretical conformational (A and B) properties of the 2-substituted benzo-1,3-tellurazoles. The theoretical and experimental (from X-ray) distances d_{1-3} between the Te atom and the nearest neighbouring atom of the 2-substituent is reported.

Derivatives		Distance [Å]					
	R	d_1		d_2		d_3	
		Exptl.	Calcd.	Exptl.	Calcd.	Exptl.	Calcd.
11$_{Te}$	^{i}Bu	3.278	3.192	3.033	3.072	–	–
12$_{Te}$	Ph	3.307	3.187	2.945	2.753	–	–
14$_{Te}$	Furanyl	3.272	3.342	–	–	3.149 (X=O)	3.250 (X=O)
15$_{Te}$	Thiophenyl	3.266	3.341	3.072	3.145	–	–
16$_{Te}$	4-Pyridyl	3.261	3.341	2.936	2.915	–	–
17$_{Te}$	3-Pyridyl	3.263	3.338	2.904	2.917	–	–
18$_{Te}$	2-Pyridyl	3.378	3.354	–	–	2.976 (X=N)	3.126 (X=N)

Table 5. ESP values for the benzo-1,3-chalcogenazoles derivatives. Y=Se or Te; X=O, N or S (heteroatom stopper).

Molecule	R	Y	$V_{S,max}$ [kcal mol^{-1}]			
			σ-hole(α)	N	σ-hole(β)	X
–	H	Se	+18.8	−29.2	+23.0	–
–		Te	+21.3	−27.9	+24.5	–
11$_{Se}$	^{i}Bu	Se	+14.1	−28.9	+16.6	–
11$_{Te}$		Te	+17.2	−20.3	+20.2	–
12$_{Se}$	Ph	Se	+15.7	−22.7	+14.4	–
12$_{Te}$		Te	+19.0	−21.0	+19.8	–
14$_{Se}$	Furanyl	Se	+16.4	−25.8	–	−9.4
14$_{Te}$		Te	+19.4	−24.5	+10.3	−7.5
15$_{Se}$	Thiophenyl	Se	+17.2	−27.0	+15.7	−15.7
15$_{Te}$		Te	+20.4	−25.1	+22.0	−15.7
16$_{Se}$	4-Pyridyl	Se	+20.5	−18.5	+18.2	−33.9
16$_{Te}$		Te	+23.5	−16.9	+24.1	−33.9
17$_{Se}$	3-Pyridyl	Se	+19.1	−21.1	+18.9	−33.9
17$_{Te}$		Te	+21.6	−19.8	+22.6	−33.9
18$_{Se}$	2-Pyridyl	Se	+14.1	−22.3	–	−23.2
18$_{Te}$		Te	+16.6	−21.6	–	−18.2

Steric control of the σ-hole recognition

As anticipated in the introductory section, this work was inspired by the solid-state organization of 2-phenyl-benzotellurazole **12**$_{Te}$ (Figure 7b),[32] in which supramolecular wires are formed through chalcogen bonding interactions ($d_{N\cdots Te}$ = 3.43 Å).

Colourless crystals of Se analogue **12**$_{Se}$ could also be easily obtained from slow evaporation of a $CHCl_3$ solution (Figure 7a). As far as it concerns the chalcogenazole heterocycle, molecule **12**$_{Se}$ displays significantly shorter Se–C bonds (≈1.90 vs. ≈2.10 Å) and C–*N*–C angle (112.8 vs. 116.9°), but a larger C–Se–C angle (84.2 and 78.6°) than those of Te-containing molecule **12**$_{Te}$. These structural characteristics are similar in all the analysed benzo-1,3-chalcogenazoles. As it was observed for the Te derivative, molecule **12**$_{Se}$ also arranges as rod-like polymers in which the benzo-1,3-chalcogenazole units are connected to each other through N···Se interactions (intermolecular $d_{N\cdots Se}$ = 3.36 Å), involving the chalcogen σ-hole(α) and the chalcogenazole N atom. In both cases, the 2-Ph substituent adopts an out-of-plane conformation (conformation A, Table 4) with respect to the benzo-1,3-chalcogenazole, featuring interplanar angles of about 25° and 31° for the Se and Te derivatives, respectively. To shed further light on the structural properties of molecules **12**$_Y$, we compared the molecular conformation in the crystal with that deriving from DFT minimization in the vacuum (Table 4). As one can clearly see, in all cases the theoretical optimization feature a planar conformation as the most stable, thus rejecting the initial hypothesis for which an electrostatic repulsion could exist between the nearest phenyl C–H and the σ-hole(β). However, a closer analysis of the crystal structure suggests that the non-planar conformation likely originates from the presence of double C–H···Y interactions (see Figure 7c for the Te case: $d_{C-H\cdots Y}$ = 2.959 and 3.072 Å), which clamps the chalcogen atoms along the supramolecular wiring direction. The C–H···Y interactions are established between positively charged hydrogen atoms and the negative region of the electrostatic surface potential encircling the chalcogen atom. These interactions are more evident with the Te atom. Replacement of the phenyl ring by an alkyl moiety did not alter the recognition properties of the benzo-1,3-chalcogenazole ring. In fact, X-ray analysis of a crystal of 2-isobutyl-substituted benzotellurazole **11**$_{Te}$ (see Figure S4 in the Supporting Information) displays the polymeric arrangement held by N···Te contacts ($d_{N\cdots Te}$ = 3.23 Å) through the σ-hole(α).

It is clear that for this molecular series, the adopted conformation (conformation A, Table 4) brings a C–H bond in close proximity to the chalcogen atom, hindering the access to the σ-hole(β). Thus, the C–H bond on the α side being more distant from the chalcogen atom than that on β (DFT values: d_1 = 3.192 and 3.187 Å and d_2 = 3.033 and 2.753 Å for **11**$_{Te}$ and **12**$_{Te}$, respectively, Table 4), the chalcogen recognition preferentially occurs at the σ-hole(α).

Barring the σ-hole through intramolecular SBIs: the σ-hole stopper

Colourless and beige crystals suitable for X-ray analysis were instead obtained for 2-furanyl benzo-1,3-chalcogenazole **14**$_{Se}$ and **14**$_{Te}$ by slow evaporation of a $CHCl_3$ solution (Figure 8).

In both cases the molecule adopts a planar conformation (conformation B, Table 4), in which the furanyl substituent is

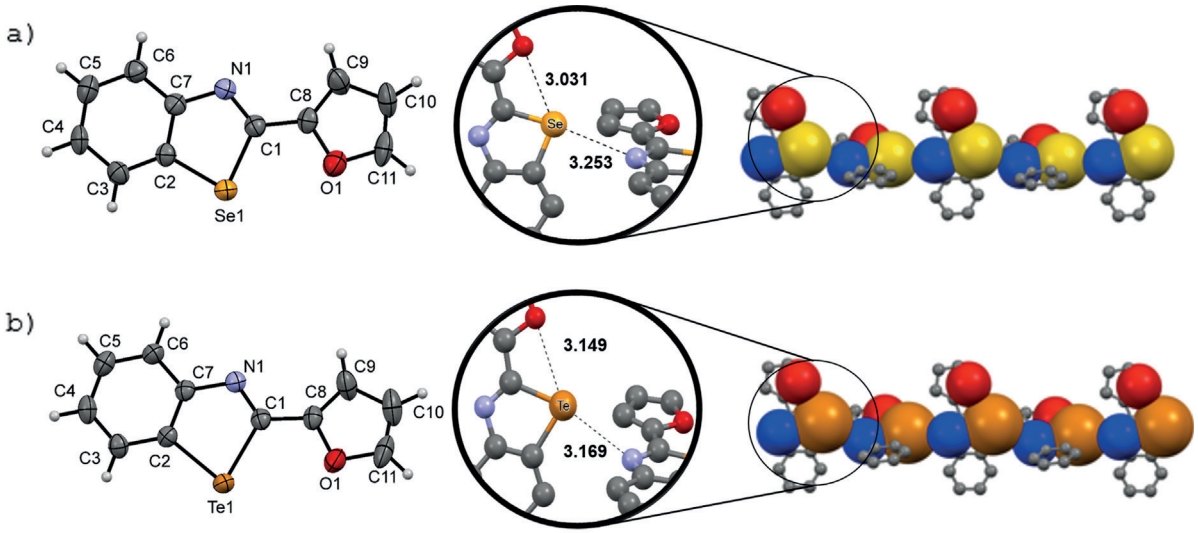

Figure 8. Ortep (left) and ball-stick/space-filling (right) representations of the crystal structure of a) $\mathbf{14_{Se}}$ and b) $\mathbf{14_{Te}}$ evidencing the supramolecular wiring motif (the N···Y contacts are viewed with the space-filling model). Distances in Å between the chalcogen atom and the SBI donor atoms are highlighted in the inset circles. Space groups: $P2_1/c$ ($\mathbf{14_{Se}}$) and *Pbca* ($\mathbf{14_{Te}}$). Atom colours: blue N, red O, ochre Te, yellow Se, grey C.

essentially coplanar (interplanar angles: 1.45 and 6.98° for $\mathbf{14_{Se}}$ and $\mathbf{14_{Te}}$, respectively) with the bicyclic benzo-1,3-chalcogenazole. Detailed analysis of the crystal structure showed that short intramolecular O···Y contacts are established ($d_{O\cdots Te}=3.03$ and 3.15 Å for $\mathbf{14_{Se}}$ and $\mathbf{14_{Te}}$, respectively, Table 5) between the furanyl O atom and the chalcogen σ-hole(β). As visualized in Table S14 (see the Supporting Information), this causes a complete ($\mathbf{14_{Se}}$, $V_{s,max} \approx 0$) or partial ($\mathbf{14_{Te}}$, $V_{s,max}=+10.3$ kcal mol^{-1}) occlusion of the σ-hole(β). As a result, molecules $\mathbf{14_{Se}}$ and $\mathbf{14_{Te}}$ feature only one electron-deficient σ-hole region on the α side ($V_{s,max}=+16.4$ and $+19.4$ kcal mol^{-1}, respectively, see Table 5).

It is thus through this σ-hole(α) that molecules $\mathbf{14_Y}$ can develop into supramolecular wires by N···Y SBIs ($d_{N\cdots Y}=3.25$ and 3.17 Å, for the Se and Te derivatives, respectively). Crystals suitable for X-ray analysis were also obtained for 2-thiophenylbenzochalcogenazole analogues $\mathbf{15_Y}$ (Figure 9). Although the resolutions of the X-ray structures is slightly inferior if compared to those of other derivatives, the data clearly display that both molecules adopt a flat conformation A (Table 4), in which the two chalcogen atoms are facing opposite sides, likely governed by N···S contacts ($d_{N\cdots S}=2.99$–3.02 for $\mathbf{15_{Se}}$ and 2.92–3.01 for $\mathbf{15_{Te}}$). The crystals of molecule $\mathbf{15_{Se}}$ only display the presence of discrete trimeric clusters held together by double N···Se interactions that, sandwiching the Se atom ($d_{N\cdots Se}=3.22$ and 3.43 Å) through its two σ-holes, form a three-atom chalcogen bonding motif (e.g., N···(α)Se(β)···N). Although the Te analogue ($\mathbf{15_{Te}}$) also forms three-atom chalcogen bonding motifs (N···(α)Te(β)···N, $d_{N\cdots Te}=3.11$ and 3.37 Å, respectively), the clusters are bridged by an additional N···Te contact ($d_{N\cdots Te}=3.42$ Å), ultimately forming a supramolecular wire at the solid state. Notably, because of the larger angles of the five-member rings at the 2-position, the σ-hole(β) is not barred by the furanyl C–H bonds ($d_{C-H\cdots Te}=3.072$ Å) and thus it results available for establishing a SBI (Table 4). 2-Pyrid-2′-yl benzo-1,3-chalcogenazoles $\mathbf{18_Y}$ display similar conformational properties (Figure 10) as those of the furanyl derivatives, namely, a co-planarity (conformation B, Table 4) between the pyridyl and the bicyclic benzo-1,3-chalcogenazole moiety (interplanar angles for the two crystallographically independent molecules: 3.2 and 5.5° for $\mathbf{18_{Se}}$ and 4.4 and 5.0° for $\mathbf{18_{Te}}$). As one can clearly discern from the X-ray crystal structure, an intramolecular N···Y contact established between the N atom of the pyridyl ring and the chalcogen σ-hole(β) is observed in both derivatives ($d_{N\cdots Te}=2.93$ and 3.02 Å for $\mathbf{18_{Se}}$ and 2.86 and 3.09 Å for $\mathbf{18_{Te}}$), causing the complete occlusion of the relevant σ-hole ($V_{s,max}=0$, Table 5 and Table S14 of the Supporting Information). As a result, only the chalcogen σ-hole(α) can engage intermolecular N···Y SBIs with the N atom ($d_{N\cdots Te}=3.33$ and 3.23 Å, for the Se and Te derivatives, respectively) to form the characteristic wire-like organization.

Triggering the wiring motif with a tethering moiety: Overcoming the chalcogenazole nitrogen atom

In all the cases discussed in the previous sections, the polymeric structures are triggered by intermolecular N···Y SBIs established through the N atom of the chalcogenazoles. However, when 2-pyrid-4′-yl benzotellurazole $\mathbf{16_{Te}}$ was crystallized, supramolecular wires featuring N···Te interactions (Figure 11) are formed involving the pyridyl N atom and the Te σ-hole(α) ($d_{N\cdots Te}=3.29$ Å).

Again, no contacts through the σ-hole(α) have been observed, most likely due to the steric hindrance exerted by the neighbouring C–H function of the pyridyl ring (conformation A, Table 4, $d_{C-H\cdots Te}=2.915$ Å). Interestingly, no N···Se contacts have been observed in the solid state for Se analogue $\mathbf{16_{Se}}$. Rather, only C–H···π and π–π interactions seem to rule the crystal organization of this molecule (Figure 11). The X-ray structure of tellurazole $\mathbf{17_{Te}}$ shows the formation of supramolecular polymers, in which the Te atoms are engaged in

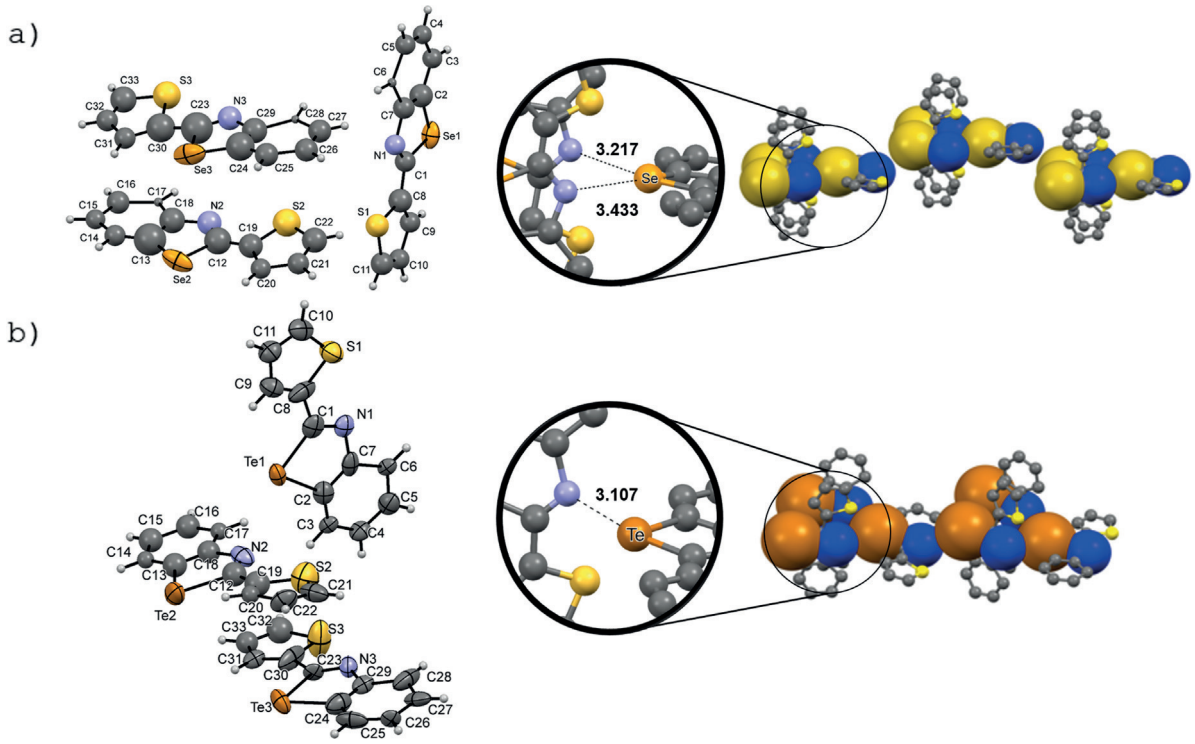

Figure 9. Ortep (left) and ball-stick (right) representations of the crystal structure of a) $\mathbf{15}_{Se}$ and b) $\mathbf{15}_{Te}$. Whereas disconnected trimeric clusters are formed at the solid state for $\mathbf{15}_{Se}$, molecule $\mathbf{15}_{Te}$ organizes into supramolecular polymers, alternating N···Te and N···Te···N contacts (the N···Y contacts are viewed with the space-filling model). Distances in Å between the chalcogen atom and the SBI donor atoms are highlighted in the inset circles. Space groups: $P2_1/c$ for both structures. Atom colours: blue N, bright yellow S, ochre Te, yellow Se, grey C. Three crystallographically independent molecules are found the unit cell for both benzochalcogenazoles.

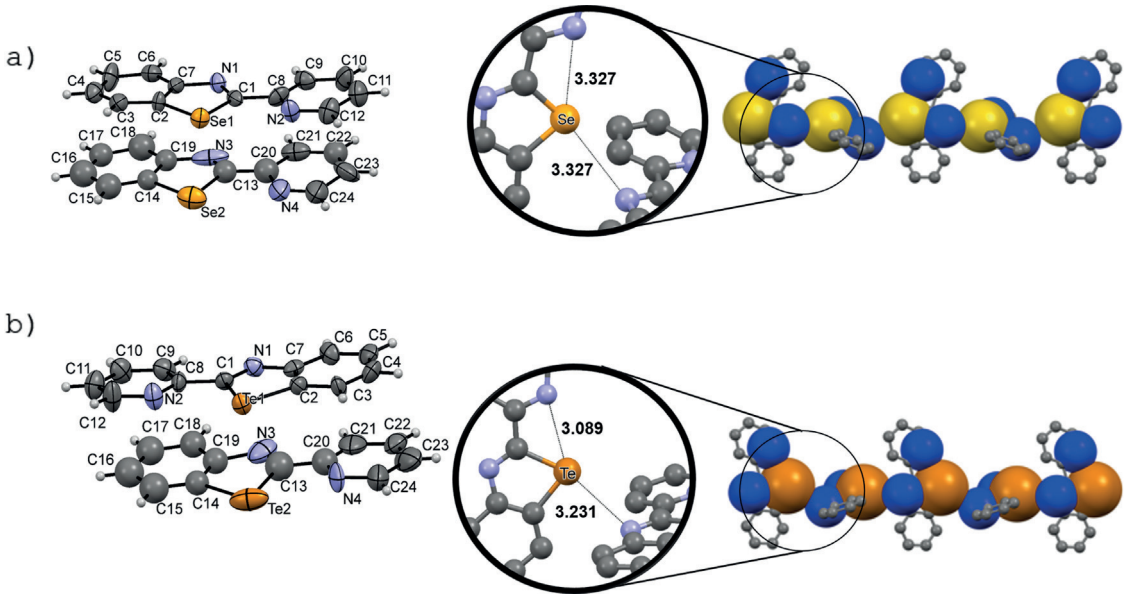

Figure 10. Ortep (left) and ball-stick/space-filling (right) representations of the crystal structure of a) $\mathbf{18}_{Se}$ and b) $\mathbf{18}_{Te}$. Both crystals evidence the wire-like organization and the conformational properties as exerted by the N···Y SBIs (the N···Y contacts are viewed with the space-filling model). Distances in Å between the chalcogen atom and the SBI donor atoms are highlighted in the inset circles. Space groups: $Pca2_1$ for both structures. Atom colours: blue N, ochre Te, yellow Se, grey C. Two crystallographically independent molecules are found the unit cell for both benzochalcogenazoles.

three-atom N···(α)Te(β)···N bonding motifs (Figure 12b) with the pyridyl and tellurazole moieties at the σ-hole(α) and σ-hole(β) sites, respectively ($d_{N\cdots Te}$ = 3.51 and 3.42 Å). Again, no N···Se contacts have been found for Se analogue $\mathbf{17}_{Se}$ (Figure 12a).

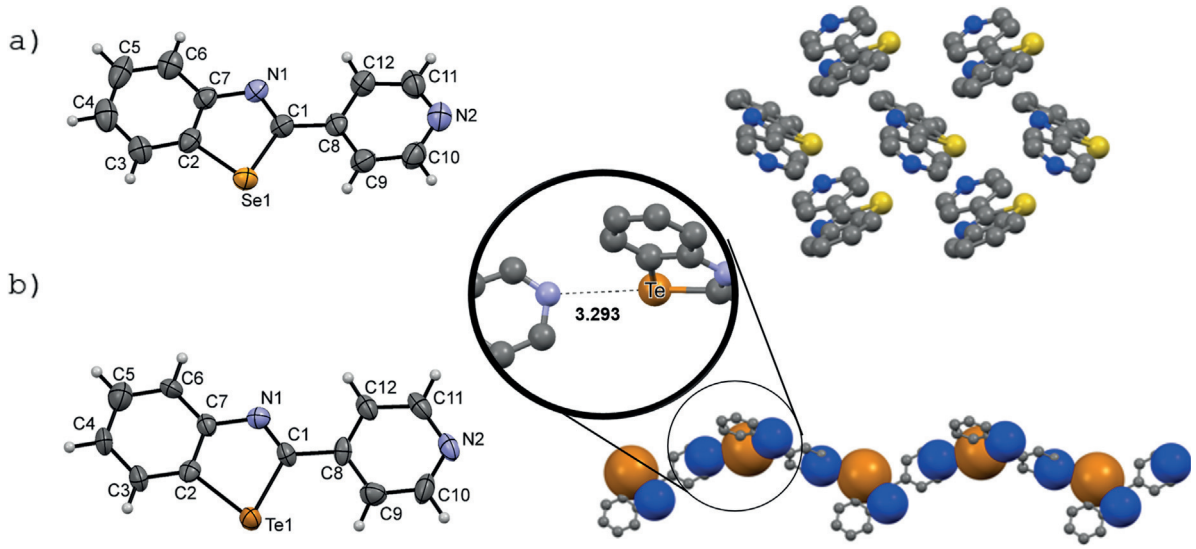

Figure 11. Ortep (left) and ball-stick/space-filling (right) representation of the crystal structure of a) $\mathbf{16}_{Se}$ and b) $\mathbf{16}_{Te}$. Only molecule $\mathbf{16}_{Te}$ forms supramolecular wires, this time tethered the pyridyl ring. Distances in Å between the chalcogen atom and the SBI donor atoms are highlighted in the inset circle. Space groups: $P2_1$ ($\mathbf{16}_{Se}$) and *Cc* ($\mathbf{16}_{Te}$). Atom colours: blue N, ochre Te, yellow Se, grey C.

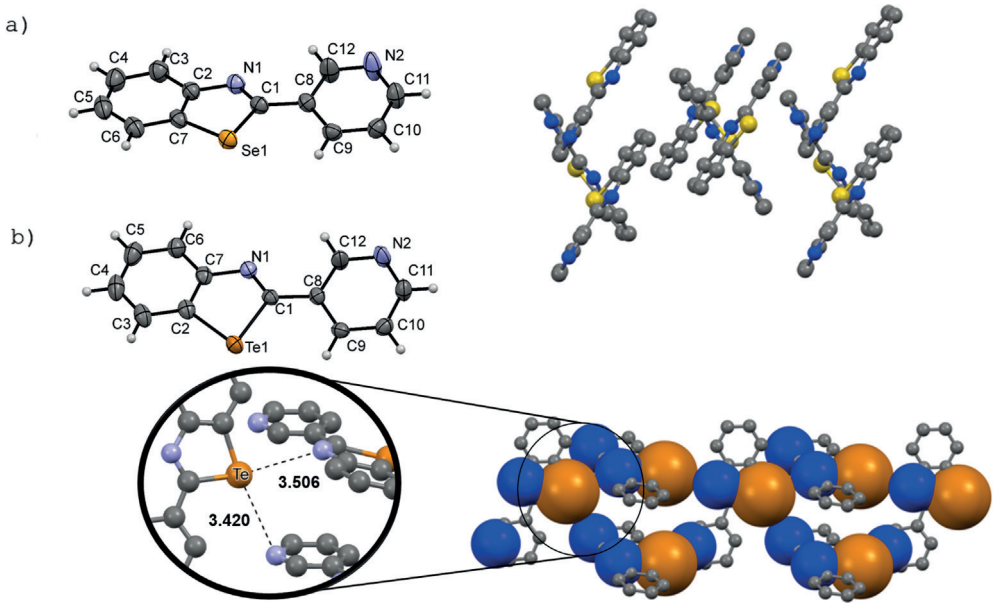

Figure 12. Ortep and ball-stick/space-filling representations of the crystal structure of a) $\mathbf{17}_{Se}$ and b) $\mathbf{17}_{Te}$ (the N···Y contacts are viewed with the space-filling model only for $\mathbf{17}_{Te}$). Distances in Å between the chalcogen atom and the SBI donor atoms are highlighted in the inset circle. Space group: $P2_1/c$ for both structures. Atom colours: blue N, ochre Te, yellow Se, grey C.

Conclusion

We have developed a versatile four-step synthesis of 2-substituted benzo-1,3-selenazoles and tellurazoles starting from 2-bromoaniline. The mild reaction conditions, simple procedure and high yields make this a valuable approach for preparing benzo-1,3-chalcogenazoles bearing a large variety of different substituents (e.g., alkyl, alkenyl, phenyl, furanyl, thiophenyl, pyridyl and ferrocenyl groups) at the 2-position. The principle of exploiting the benzo-1,3-chalcogenazole as self-assembling units to produce controlled organic networks at the solid-state through SBIs has been demonstrated with a large number of examples. In particular, by programming the recognition properties of the chalcogen σ-hole sites and of the basic chalcogen-bonding acceptor atom through the selection of suitable 2-substituents, we gain control of the wiring arrangement of the benzo-1,3-chalcogenazoles at the solid state. With such building units, when the overall assembly process is symmetry-conserved; the final supramolecular framework depends upon the type of the chalcogen bonding donor and the symmetry of its recognition σ-hole sites. With this simple governing principle and the large library of stable benzochalcogenazole modules that could be envisaged, it will be possible to engineer a great variety of materials featuring a series of tunable organi-

zations with tremendous variations in the optoelectronic properties and thus device application.

Acknowledgements

D.B. gratefully acknowledges the FRS-FNRS, the Science Policy Office of the Belgian Federal Government (BELSPO-IAP 7/05 project). A.K. thanks the FNRS for his research associate position. The authors thank the physical chemistry and characterization (PC^2) at the UNamur for the X-ray. Calculations were performed on the computer of the 'Consortium des Equipement de Calcul Intensif' and mostly those of the Technological Platform of High-Performance Computing, for which the authors acknowledge the financial support of the FNRS-FRFC (conventions No. 2.4.617.07.F) and the University of Namur.

Keywords: chalcogens · selenium · self-assembly · supramolecular chemistry · tellurium · UV/Vis spectroscopy

[1] T. Chivers, R. S. Laitinen, *Chem. Soc. Rev.* **2015**, *44*, 1725 – 1739.
[2] a) N. W. Alcock, *Adv. Inorg. Chem. Radiochem*. **1972**, *15*, 1 – 58; b) C. E. Housecroft, A. G. Sharpe, *Inorganic Chemistry,* 4th ed., Pearson Education Ltd., Harlow, England, **2012**.
[3] W.-W. duMont, C. G. Hrib, in *Handbook of Chalcogen Chemistry: New Perspectives in Sulfur, Selenium and Tellurium, Vol. 2*, 2nd ed. (Eds.: F. A. Devillanova, W.-W. d. Mont), RSC Publishing, London, **2013**, pp. 273 – 316.
[4] A. F. Cozzolino, P. J. W. Elder, I. Vargas-Baca, *Coord. Chem. Rev.* **2011**, *255*, 1426 – 1438.
[5] T. M. Beale, M. G. Chudzinski, M. G. Sarwar, M. S. Taylor, *Chem. Soc. Rev.* **2013**, *42*, 1667 – 1680.
[6] P. Metrangolo, F. Meyer, T. Pilati, G. Resnati, G. Terraneo, *Angew. Chem. Int. Ed.* **2008**, *47*, 6114 – 6127; *Angew. Chem.* **2008**, *120*, 6206 – 6220.
[7] P. Metrangolo, G. Resnati, *Science* **2008**, *321*, 918 – 919.
[8] L. C. Gilday, S. W. Robinson, T. A. Barendt, M. J. Langton, B. R. Mullaney, P. D. Beer, *Chem. Rev.* **2015**, *115*, 7118 – 7195.
[9] M. Erdélyi, *Chem. Soc. Rev.* **2012**, *41*, 3547 – 3557.
[10] M. J. Langton, S. W. Robinson, I. Marques, V. Félix, P. D. Beer, *Nat. Chem.* **2014**, *6*, 1039 – 1043.
[11] R. Bertani, P. Sgarbossa, A. Venzo, F. Lelj, M. Amati, G. Resnati, T. Pilati, P. Metrangolo, G. Terraneo, *Coord. Chem. Rev.* **2010**, *254*, 677 – 695.
[12] G. Cavallo, P. Metrangolo, T. Pilati, G. Resnati, M. Sansotera, G. Terraneo, *Chem. Soc. Rev.* **2010**, *39*, 3772 – 3783.
[13] E. Parisini, P. Metrangolo, T. Pilati, G. Resnati, G. Terraneo, *Chem. Soc. Rev.* **2011**, *40*, 2267 – 2278.
[14] R. Berger, G. Resnati, P. Metrangolo, E. Weber, J. Hulliger, *Chem. Soc. Rev.* **2011**, *40*, 3496 – 3508.
[15] M. Cametti, B. Crousse, P. Metrangolo, R. Milani, G. Resnati, *Chem. Soc. Rev.* **2012**, *41*, 31 – 42.
[16] P. Metrangolo, G. Resnati, *Nat. Chem.* **2012**, *4*, 437 – 438.
[17] C. Cohen-Addad, M. S. Lehmann, P. Becker, L. Parkanyi, A. Kalman, *J. Chem. Soc. Perkin Trans. 2* **1984**, 191 – 196.
[18] J. Fanfrlík, A. Prada, Z. Padelkova, A. Pecina, J. Machacek, M. Lepsik, J. Holub, A. Ruzicka, D. Hnyk, P. Hobza, *Angew. Chem. Int. Ed.* **2014**, *53*, 10139 – 10142; *Angew. Chem.* **2014**, *126*, 10303 – 10306.
[19] R. E. Rosenfield, Jr., R. Parthasarathy, J. D. Dunitz, *J. Am. Chem. Soc.* **1977**, *99*, 4860 – 4862.
[20] T. N. G. Row, R. Parthasarathy, *J. Am. Chem. Soc.* **1981**, *103*, 477 – 479.
[21] G. E. Garrett, G. L. Gibson, R. N. Straus, D. S. Seferos, M. S. Taylor, *J. Am. Chem. Soc.* **2015**, *137*, 4126 – 4133.
[22] E. Alikhani, F. Fuster, B. Madebene, S. J. Grabowski, *Phys. Chem. Chem. Phys.* **2014**, *16*, 2430 – 2442.
[23] M. E. Brezgunova, J. Lieffrig, E. Aubert, S. Dahaoui, P. Fertey, S. Lebègue, J. G. Angyan, M. Fourmigué, E. Espinosa, *Cryst. Growth Des.* **2013**, *13*, 3283 – 3289.
[24] T. Clark, M. Hennemann, J. S. Murray, P. Politzer, *J. Mol. Model.* **2007**, *13*, 291 – 296.
[25] A. F. Cozzolino, I. Vargas-Baca, S. Mansour, A. H. Mahmoudkhani, *J. Am. Chem. Soc.* **2005**, *127*, 3184 – 3190.
[26] S. Tsuzuki, N. Sato, *J. Phys. Chem. B* **2013**, *117*, 6849 – 6855.
[27] W. Wang, B. Ji, Y. Zhang, *J. Phys. Chem. A* **2009**, *113*, 8132 – 8135.
[28] A. F. Cozzolino, J. F. Britten, I. Vargas-Baca, *Cryst. Growth Des.* **2006**, *6*, 181 – 186.
[29] N. W. Alcock, *Adv. Inorg. Chem. Radiochem.* **1972**, *15*, 1 – 58.
[30] R. N. Behera, A. Panda, *Comput. Theor. Chem.* **2012**, *999*, 215 – 224.
[31] A. F. Cozzolino, I. Vargas-Baca, *J. Organomet. Chem.* **2007**, *692*, 2654 – 2657.
[32] A. E. Mistryukov, I. D. Sadekov, V. S. Sergienko, G. M. Abakarov, M. A. Porai-Koshits, A. A. Shneider, A. D. Garnovskii, *Chem. Heterocycl. Compd.* **1989**, *25*, 1407 – 1409.
[33] A. Kremer, C. Aurisicchio, F. De Leo, B. Ventura, J. Wouters, N. Armaroli, A. Barbieri, D. Bonifazi, *Chem. Eur. J.* **2015**, *21*, 15377 – 15387.
[34] A. F. Cozzolino, P. J. W. Elder, L. M. Lee, I. Vargas-Baca, *Can. J. Chem.* **2013**, *91*, 338 – 347.
[35] S. M. Huber, E. Jimenez-Izal, J. M. Ugalde, I. Infante, *Chem. Commun.* **2012**, *48*, 7708 – 7710.
[36] L. P. Wolters, F. M. Bickelhaupt, *ChemistryOpen* **2012**, *1*, 96 – 105.
[37] A. F. Cozzolino, I. Vargas-Baca, *Cryst. Growth Des.* **2011**, *11*, 668 – 677.
[38] L. P. Wolters, P. Schyman, M. J. Pavan, W. L. Jorgensen, F. M. Bickelhaupt, S. Kozuch, *WIREs Comput. Mol. Sci.* **2014**, *4*, 523 – 540.
[39] P. Politzer, J. S. Murray, T. Clark, *Phys. Chem. Chem. Phys.* **2013**, *15*, 11178 – 11189.
[40] M. Mbuyi, M. Evers, G. Tihange, A. Luxen, L. Christiaens, *Tetrahedron Lett.* **1983**, *24*, 5873 – 5876.
[41] T. Junk, K. J. Irgolic, *Phosphorus Sulfur Relat. Elem*. **1988**, *38*, 121 – 135.
[42] G. M. Abakarov, A. A. Shabson, I. D. Sadekov, A. D. Garnovskii, V. I. Minkin, *Chem. Heterocycl. Compd.* **1988**, *24*, 232 – 234.
[43] G. M. Abakarov, A. A. Shabson, I. D. Sadekov, A. D. Granovskii, V. I. Minkin, *Khim. Geterotsikl. Soedin.* **1988**, 276 – 278.
[44] C. S. Radatz, D. Alves, P. H. Schneider, *Tetrahedron* **2013**, *69*, 1316 – 1321.
[45] C. Schwartz Radatz, D. S. Rampon, R. A. Balaguez, D. Alves, P. H. Schneider, *Eur. J. Org. Chem.* **2014**, 6945 – 6952.
[46] R. A. Balaguez, R. Kruger, C. S. Radatz, D. S. Rampon, E. J. Lenardao, P. H. Schneider, D. Alves, *Tetrahedron Lett.* **2015**, *56*, 2735 – 2740.
[47] S. Redon, Y. Kabri, M. D. Crozet, P. Vanelle, *Tetrahedron Lett.* **2014**, *55*, 5052 – 5054.
[48] T. Su, S. Xie, B. Li, J. Yan, L. Huang, X. Li, *Synlett* **2015**, *26*, 215 – 220.
[49] I. D. Sadekov, G. M. Abakarov, A. A. Shneider, S. G. Kuren, A. G. Starikov, A. D. Garnovskii, V. I. Minkin, *Chem. Heterocycl. Compd.* **1989**, *25*, 103 – 108.
[50] P. R. Mallikarachy, H. O. Brotherton, F. R. Fronczek, T. Junk, *J. Heterocycl. Chem.* **2005**, *42*, 243 – 247.
[51] N. C. McMullen, F. R. Fronczek, T. Junk, *J. Heterocycl. Chem.* **2013**, *50*, 120 – 124.
[52] I. G. Borodkina, A. I. Uraev, G. S. Borodkin, I. D. Sadekov, A. D. Garnovskii, V. I. Minkin, *Russ. J. Gen. Chem.* **2003**, *73*, 1810 – 1814.
[53] I. G. Borodkina, A. I. Uraev, G. S. Borodkin, I. D. Sadekov, A. D. Garnovskii, V. I. Minkin, *Zh. Obshch. Khim.* **2003**, *73*, 1910 – 1914.
[54] T. Annaka, N. Nakata, A. Ishii, *Organometallics* **2015**, *34*, 1272 – 1278.
[55] G. He, W. Torres Delgado, D. J. Schatz, C. Merten, A. Mohammadpour, L. Mayr, M. J. Ferguson, R. McDonald, A. Brown, K. Shankar, E. Rivard, *Angew. Chem. Int. Ed.* **2014**, *53*, 4587 – 4591; *Angew. Chem.* **2014**, *126*, 4675 – 4679.
[56] G. He, W. Torres Delgado, D. J. Schatz, C. Merten, A. Mohammadpour, L. Mayr, M. J. Ferguson, R. McDonald, A. Brown, K. Shankar, E. Rivard, *Angew. Chem.* **2014**, *126*, 4675 – 4679.
[57] M. Kolar, J. Hostas, P. Hobza, *Phys. Chem. Chem. Phys.* **2014**, *16*, 9987 – 9996.
[58] J. S. Murray, P. Lane, P. Politzer, *Int. J. Quantum Chem.* **2007**, *107*, 2286 – 2292.

Received: October 28, 2015
Published online on February 22, 2016